# Electron ejection from clean metallic surfaces upon charged particle impact

J. Berakdar[1] and M. P. Das[2]
[1]*Max-Planck Institute of Microstructure Physics, Weinberg 2, 06120 Halle, Germany*
[2]*Theoretical Physics Department, Research School of Physical Sciences and Engineering, Australian National University, Canberra, Australian Capital Territory 0200, Australia*
(Received 12 February 1997)

In this work we present a theoretical treatment of electron ejection from a clean metallic semi-infinite solid with an ideal orthorhombic Bravais lattice following the impact of moderately fast charged particles with respect to the Fermi momentum of the initially bound electron. For an aluminum semi-infinite solid target multiple differential cross sections have been evaluated using a jellium-type wave function of the undisturbed surface in the initial state. Image-charge final-state electron-surface interactions have been included as well as the scattering of the projectile from the multicenter bulk potential. From a kinematic analysis of the process various ionization mechanisms are inferred and confirmed by the present dynamical model. [S1050-2947(97)05408-5]

PACS number(s): 79.20.Kz

## I. INTRODUCTION

The pathways for the simultaneous emission of two electrons from atomic and molecular systems upon electron impact [hereafter referred to as the $(e,2e)$ process] have been investigated thoroughly [1–3]. The complexity of this reaction is already revealed in the simplest case of the low-energy electron-impact ionization of atomic hydrogen where final-state interactions of the escaping particles strongly modify the observed electron spectra [4,5]. Hence a realistic approximate eigenfunction of the nonseparable three-body Hamiltonian is needed. Although such experiments using thin solid films have been conducted [7] shortly after their atomic counterpart [8,9], the study of the dynamics of ionization of solid surfaces upon charged particle impact is still in its infancy. In general, a theoretical description of this process from solid targets has to deal with various aspects of the beam-solid interactions. A charged projectile impinging on a metallic target, which is the subject of this work, leads to a charge-density fluctuation in the solid. Asymptotically, this causes an image-charge distortion of the incoming and outgoing particles [6]. Furthermore, the motion of vacuum electrons is periodically distorted by the interaction with the bulk potential [10,11]. In addition, the electronic beams are attenuated by the incoherent generation of optical phonons. Interactions with acoustic phonons lead to spreading of these beams [10,12,13]. The excitation of collective modes during the collision process poses an additional obstacle for theoretical treatment, in particular if the ionization event takes place in an inner band with simultaneous plasmon generation. The description of the elastic and inelastic multiple-scattering events from the multicenter solid potential is a further complication for theory. The strength of the above-mentioned interactions is very much dependent on the interaction time of the projectile-solid scattering system and hence on the velocity vectors of the incoming and escaping particles. In fact, in a transmission mode $(e,2e)$ scattering from thin films, all above-listed processes can be neglected for high energetic (in the keV regime) incoming and outgoing electrons under Bethe-ridge kinematics [14–16]. The vacuum electrons are then described by undistorted plane waves. The secondary electron is knocked out by a direct encounter with the projectile, while all other degrees of freedom of the solid remain ''frozen'' [17–19,15]. Under these circumstances the measured cross section can be related to the spectral momentum density of the initially bound electron [15,16]. This fact has been employed for the experimental investigation of the band structure of a variety of solid targets (see [15,16,20] and references therein). The corresponding theory [21,22] deals essentially with the band structure of the solid rather than scattering dynamics. The successful description of the spectral electron-momentum densities underlines the validity of this one-step impulsive plane-wave approximation (IPWA) in this case. However, even at higher energies, the IPWA breaks down in the reflection mode since in this case, at least, a two-step mechanism is required for the ejection of the electrons. Nevertheless, as shown in Refs. [23,24], some information on the target band structure can still be extracted from these experiments even at moderate electron energies. With decreasing energies of the vacuum electrons the above-mentioned electron-solid interactions become relevant.

A series of $(e,2e)$ measurements from W(001) and LiF have been conducted at energies close to the vacuum threshold and in the normal-incidence, back-reflection geometry. Surprisingly, the qualitative features of the observed spectra coincide with the predictions of a crude kinematic model [25–27]. To explain these experiments sophisticated low-energy quantum-mechanical calculations have been performed recently [28].

The aim of this paper is to investigate the dominant mechanisms for the electron ejection from a metallic surface at moderate energies (several times the Fermi energy). The feasibility of such experiments with sufficient angular and energy resolutions has been demonstrated [23,24]. The fundamental underlying approximation of the present study is the assumption that the degrees of freedom of the projectile can be decoupled from those of the target. This is justified since we assumed the momenta of the incoming and outgoing electron to be considerably larger than the Fermi momentum. In order to obtain analytical results that can be simply

 

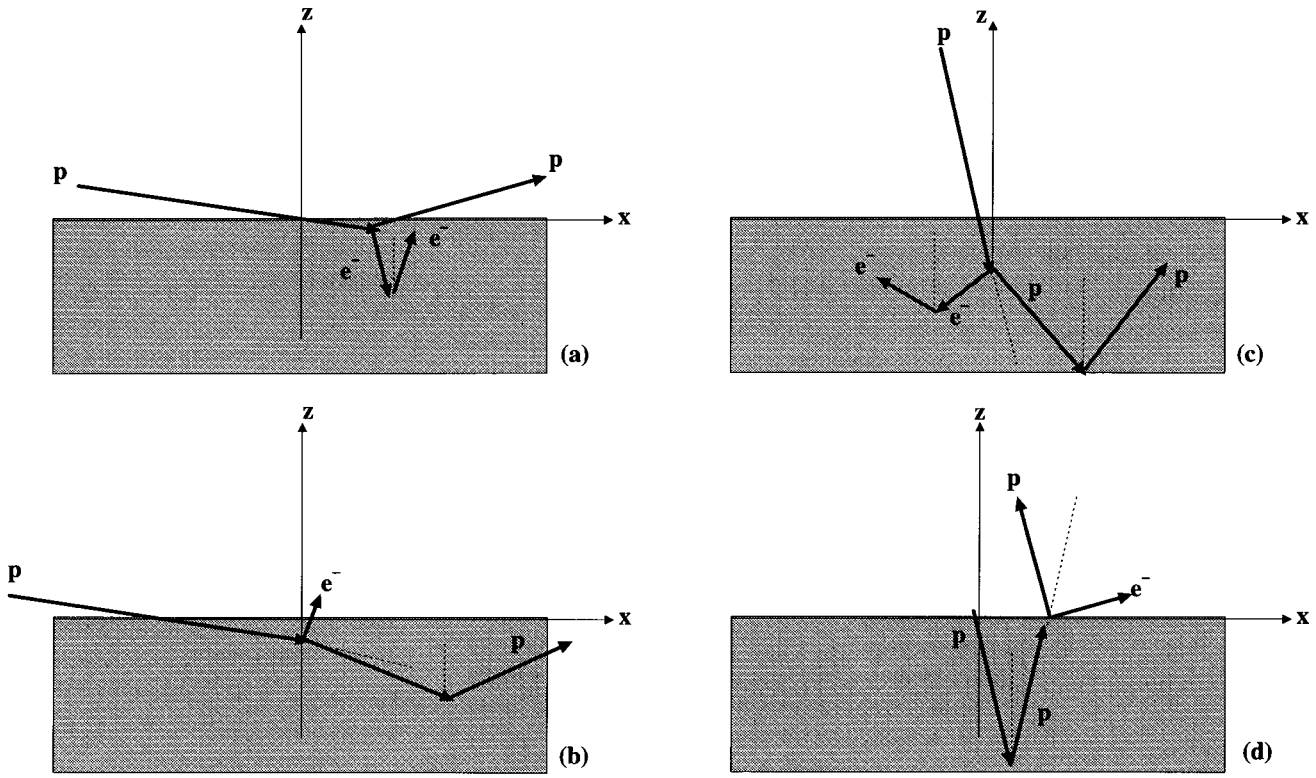


FIG. 1. Schematic representation of the different ionization mechanisms (a)–(d) as described in the text.

analyzed, a jellium wave function of the initially bound electron is assumed. Asymptotic image-charge distortion of the vacuum electron is taken into account. In addition to the binary collision of the projectile with the bound electron, the scattering of the incident particle from the multicenter bulk potential is treated in the kinematic approximation [11,30]. A screened Coulomb muffin-tin bulk potential is adopted. The applicability of the theory is limited to the moderate electrons' energies, which allows us to neglect plasmon and phonon excitations, as described above. Within this model four possible collisional mechanisms for the ejection of electron pairs are identified (see Fig. 1). In the first process the projectile is directly transferred into the vacuum after a binary collision with the electron. The electron recoils off the ''background charged'' elastically. In the second process the electron is knocked out into the vacuum following a binary encounter with the projectile, whereas the projectile recoils off the multicenter bulk potential. In the third process the two electrons recoil off the bulk potential after a direct binary scattering. Finally, in the fourth process both electrons are ejected into the vacuum after the projectile recoils off the bulk potential. The theory is formulated for a structureless projectile of an arbitrary mass and charge. However, the assumption of negligible phonon excitation due to the projectile impact becomes questionable for energetic heavy (with respect to the ionic core) projectiles. Atomic units are used throughout.

## II. THEORETICAL FORMULATION

We consider a scattering system consisting of a projectile with charge $Z_p$ and mass $m_p$ being inelastically scattered from a clean, metallic semi-infinite solid ejecting one electron into a vacuum level of the solid. The total Hamiltonian of the projectile-solid system is

$$\mathcal{H}=H_p+H_e+W_{pe}, \tag{1}$$

where $H_e$ is the Hamiltonian of the semi-infinite solid in the absence of the projectile, $W_{pe}$ is the projectile-ejected electron interaction, and $H_p$ describes the projectile-crystal interaction and contains the plasmon and phonon modes and their interaction with the electron. To avoid difficulties associated with infinite-range potentials that lead to scattering even at an infinitely large impact parameter we assume all infinite-range interactions involved in our process to be screened at a large but finite distance. This allows us to define asymptotically unperturbed initial and final channel Hamiltonians $H_i$ and $H_f$, respectively. The initial and final-state boundary conditions are specified by eigenstates $|i\rangle,|f\rangle$ of $H_i$ and $H_f$, i.e.,

$$(H_i-E_i)|i\rangle=0, \tag{2}$$

$$(H_f-E_f)|f\rangle=0, \tag{3}$$

where $E_i,E_f$ are the corresponding asymptotic eigenenergies. The transition amplitude $T$ for the scattering system, initially prepared in the (asymptotic) state $|i\rangle$, to go over into the asymptotic final state $|f\rangle$ is determined by the prior form

$$T=\langle\Psi^-|V_i|i\rangle \tag{4}$$

or the post form

$$T=\langle f|V_f|\Psi^+\rangle. \tag{5}$$

The state vectors $|\Psi^+\rangle$ and $|\Psi^-\rangle$ are eigenstates of the total Hamiltonians $\mathcal{H}$, given by Eq. (1), with the asymptotic behavior given by $|i\rangle$ and $|f\rangle$, respectively. The $+$ $(-)$ sign refers to to incoming (outgoing) wave boundary conditions. In Eqs. (4) and (5) the perturbations $V_i$ and $V_f$ are given by

$$V_i=\mathcal{H}-H_i, \tag{6}$$

$$V_f=\mathcal{H}-H_f. \tag{7}$$

In what follows we confine the treatment to the prior form of the $T$ matrix [Eq. (4)]. Equivalent considerations apply to the post form. The eigenstate $|\Psi^-\rangle$ of $\mathcal{H}$ can be written as

$$|\Psi^-\rangle=\Omega^-|f\rangle, \tag{8}$$

where the Møller wave operator $\Omega^-$ is given by

$$\Omega^-=1+G^-V_f. \tag{9}$$

In Eq. (9) $G^-$ is the resolvent (Green operator) of the total Hamiltonian $\mathcal{H}$. Combining Eqs. (9), (8), and (4), the $T$ matrix element reads

$$T=T^{sin}+T^{mult}, \tag{10}$$

where

$$T^{sin}:=\langle f|V_i|i\rangle, \tag{11}$$

$$T^{mult}:=\langle f|V_fG^+V_i|i\rangle. \tag{12}$$

Assuming $V_i$ to be a multiple-center potential, the first term of Eq. (10), $T^{sin}$, describes the transition of the system from state $|i\rangle$ to $|f\rangle$ due to a single scattering from each individual scattering center. One-center and multicenter multiple scattering is contained in the matrix element $T^{mult}$ in Eqs. (10) and (12) since the Lippmann-Schwinger equation of the total Green operator leads to the expansion

$$T^{mult}=\left\langle f\left|V_fG_0^+\sum_{j=0}^{\infty}[VG_0^+]^j\right|i\right\rangle, \tag{13}$$

where $G_0^+$ and $V$ are the full free propagator and the total potential of the projectile-solid compound. It should be noted here that the labels $sin$ and $mult$ of the amplitudes $T^{sin}$ and $T^{mult}$ refer to single and multiple scattering specifically from the potential $V_i$. In this study we choose the asymptotic initial state as a noninteracting projectile-solid state, i.e.,

$$H_i=H_e+K_p, \tag{14}$$

where $K_p$ is the kinetic-energy operator of the projectile. Thus, according to Eq. (6), the perturbation in the initial channel can be written as

$$V_i=\mathcal{H}-H_i=W_{pe}+W_p^s+W_p^{vac}. \tag{15}$$

The operator $W_p^s$ stands for the projectile-bulk interaction and its explicit functional form is specified below. The potential $W_p^{vac}$ amounts to the asymptotic interaction of the projectile with the solid. As mentioned in the Introduction, we deal with a fast projectile with respect to the Fermi velocity so that projectile-phonon coupling is negligible (the motion of the ionic cores is very slow on the time scale of the projectile-solid interaction time). For the asymptotic final-channel Hamiltonian the following choice is appropriate:

$$H_f=K_e+K_p+W_p^{vac}+W_e^{vac}+W_{pe}. \tag{16}$$

Here the kinetic-energy operator of the secondary electron is referred to by $K_e$, whereas $W_e^{vac}$ amounts to the asymptotic final-state interaction of this electron with the semi-infinite solid. The choice (16) leads to the final-channel distortion operator

$$V_f=W_p^s+W_e^s, \tag{17}$$

where $W_e^s$ denotes the short-range interaction of the secondary electron with the surface.

## III. STRUCTURE OF THE MULTICENTER SINGLE-SCATTERING AMPLITUDE

Upon substitution of Eq. (15) into Eq. (11), the matrix element $T^{sin}$ can be decomposed into

$$T^{sin}=T_{pe}^{sin}+T_{p,s}^{sin}+T_{p,v}^{sin}, \tag{18}$$

where

$$T_{pe}^{sin}:=\langle f|W_{pe}|i\rangle, \tag{19}$$

$$T_{p,s}^{sin}:=\langle f|W_p^s|i\rangle, \tag{20}$$

$$T_{p,v}^{sin}:=\langle f|W_p^{vac}|i\rangle. \tag{21}$$

As we are dealing with a metallic semi-infinite solid we adopt a mean-field, one-particle treatment of the initially bound electron in the solid, e.g., a jellium model. Neglecting any corrections due to the finite mass of the solid with respect to $m_p$, we choose a coordinate system in which the $x$ and $y$ directions lie in the surface plane, whereas the $z$ axis is chosen as the normal of the surface pointing into the vacuum. The origin is chosen at the highest occupied electronic band at absolute zero temperature, e.g., at the jellium edge. The amplitudes, given by Eqs. (19) and (20), provide (in a perturbative sense) the first-order approximation to the matrix element $T$. The term given by Eq. (21) is less prominent since $W_p^{vac}$ is an asymptotic (image charge) perturbation. In fact, including $W_p^{vac}$ in $H_i$ [Eq. (14)] instead of $V_i$ [Eq. (15)] would lead to only a logarithmic phase modification of the plane-wave motion of the projectile. This modification is insignificant for high-velocity projectiles.

In a position-space representation the transition operator occurring in Eq. (19) has the form $W_{pe}=-Z_p/|\mathbf{r}_p-\mathbf{r}_e|$, where $\mathbf{r}_p$ and $\mathbf{r}_e$ are the position vectors of the projectile and ionized electron, respectively. In the present model, $T_{pe}^{sin}$ is an estimate for the probability of the direct transition of a delocalized electronic bound state into a vacuum state after a direct projectile-electron encounter. No effect of the periodic structure of the solid is included in Eq. (19). On the other hand, the transition amplitude $T_{p,s}^{sin}$ [Eq. (20)] is a measure for the electron-ejection probability due to an initial scattering of the projectile from the periodic potential of the solid

and a subsequent projectile-electron collision. The latter encounter is included as a final-state projectile-electron interaction, as can be seen from Eq. (16). Thus it is comprehensible that the transition amplitude $T_{p,s}^{sin}$ shows some resemblance to the low-energy electron diffraction (LEED) transition amplitude, as indicated below.

### A. Evaluation of $T_{p,s}^{sin}$

Suppose that in a scattering experiment the final-channel asymptotic vector momenta $\mathbf{k}_p, \mathbf{k}_e$ are simultaneously specified as well as the incident vector momentum $\mathbf{k}_i$ of the projectile. For simplicity we disregard for the moment the (asymptotic) image-charge (logarithmic phase) distortions of the projectile and electron motion in the final state. In the projectile case this is reasonable since we assumed fast scattered particles. Distortions of the electron's motion in the final state due to the (asymptotic) image-charge field are considered subsequently. Thus, for the moment, we neglect the potential $W_p^{vac}, W_e^{vac}$ in Eq. (16). For a given final-state energy $E_f$, the two-center Hamiltonian $H_f$ is exactly separable in the coordinate system $\mathbf{R}_- \otimes \mathbf{R}_+$, where $\mathbf{R}_- = \mathbf{r}_p - \mathbf{r}_e$ and $\mathbf{R}_+ = \mathbf{r}_p + \mathbf{r}_e$. The asymptotic state $|f\rangle$ reads

$$|f\rangle = |\mathbf{K}_+\rangle \otimes |\phi_{\mathbf{K}_-}\rangle, \tag{22}$$

where $|\mathbf{K}_+\rangle$ describes the plane-wave motion in the coordinate $\mathbf{R}_+$ with the conjugate asymptotic momentum $\mathbf{K}_+ = \mathbf{k}_p + \mathbf{k}_e$ and $|\phi_{\mathbf{K}_-}\rangle$ satisfies the Lippmann-Schwinger equation ($W_{pe}$ is assumed to be of finite range)

$$|\phi_{\mathbf{K}_-}\rangle = (1 + g_{pe}^{+} W_{pe}) |\mathbf{K}_-\rangle. \tag{23}$$

Here $|\mathbf{K}_-\rangle$ denotes a plane-wave state vector in the electron-projectile coordinate $\mathbf{R}_-$ with the corresponding conjugate momentum $\mathbf{K}_- = \mu_p(\mathbf{k}_p/m_p - \mathbf{k}_e)$, where $\mu_p = m_p/(m_p+1)$ is the electron-projectile reduced mass. In Eq. (23) $g_{pe}^{+}$ is the full propagator of the projectile-electron relative motion in the potential $W_{pe}$.

The form of the asymptotic initial-state Hamiltonian $H_i$ [Eq. (14)] implies that $|i\rangle$ can be expressed as the direct product $|i\rangle = |\mathbf{k}_i\rangle \otimes |\chi_{\mathbf{k}}\rangle$, where $|\mathbf{k}_i\rangle$ describes the free projectile motion with incident momentum $\mathbf{k}_i$ and $|\chi_{\mathbf{k}}\rangle$ is an eigenstate of the solid Hamiltonian $H_e$ with initial binding energy $\epsilon_{\mathbf{k}}$. Considering Eq. (23) and changing the representation to $\mathbf{r}_p \otimes \mathbf{r}_e$, Eq. (20) can therefore be written in the form

$$T_{p,s}^{sin} = \langle \mathbf{k}_p, \mathbf{k}_e | W_p^s | \chi_{\mathbf{k}}, \mathbf{k}_i \rangle + \langle \mathbf{k}_p, \mathbf{k}_e | W_{pe} g_{pe}^{-} W_p^s | \chi_{\mathbf{k}}, \mathbf{k}_i \rangle. \tag{24}$$

In this work we assume that the projectile-bulk periodic scattering potential depends only on $\mathbf{r}_p$ and its form will be specified below. Thus the first term in Eq. (24) involves a direct overlap of the eigenstates $|\chi_{\mathbf{k}}\rangle$ and $|\mathbf{k}_e\rangle$ of the same Hamiltonian $H_e$ with different eigenvalues $(\epsilon_{\mathbf{k}}, k_e^2/2)$ and therefore vanishes. Since the full projectile-electron propagator $g_{pe}^{-} = g_0^{-} + g_0^{-} W_{pe} g_{pe}^{-}$ enters in the second term of Eq. (24), the corresponding two-body scattering takes place an infinite number of times. In spirit of the *kinematic approximation* employed in LEED studies [11,30,29], only single scattering from each of the scattering centers is taken into account. This amounts to replacing $g_{pe}^{-}$ by $g_0^{-}$ in Eq. (24). To derive an expression for $T_{p,s}^{sin}$ we reformulate Eq. (24) as

$$T_{p,s}^{sin} = \langle \mathbf{k}_e | F | \chi_{\mathbf{k}} \rangle_{\mathbf{r}_e}, \tag{25}$$

where upon the introduction of complete sets of plane waves in the momentum space conjugate to $|\mathbf{R}_-\rangle$ the operator $F$ is given by

$$F = \int \int d^3q d^3q' \langle \mathbf{k}_p | W_{pe} | \mathbf{q}' \rangle \langle \mathbf{q}' | g_0^{-} | \mathbf{q} \rangle \langle \mathbf{q} | W_p^s | \mathbf{k}_i \rangle_{r_p}. \tag{26}$$

The term $\langle \mathbf{q}' | g_0^{-} W_p^s | \mathbf{k}_i \rangle_{r_p}$ describes the scattering of free charged particles with momentum $\mathbf{k}_i$ from the periodic potential of the solid $W_p^s$ and their free propagation into a free-particle beam with momentum $\mathbf{q}'$. This corresponds to the LEED process [29]. Thus Eq. (25) can be interpreted as follows. A beam of free particles $|\mathbf{k}_i\rangle$ scatters into a free beam of particles from the periodic potential $W_p^s$ and propagates freely to an initially bound electronic distribution of the solid, described by $|\chi_{\mathbf{k}}\rangle$. After an inelastic collision with the projectile this distribution is transferred into a free vacuum state $|\mathbf{k}_e\rangle$, whereas the projectile emerges into a free state $|\mathbf{k}_p\rangle$.

To evaluate the expression $F$ [Eq. (26)] the Fourier transform of the periodic potential $W_p^s$ is needed. Here we consider a solid with an orthorhombic Bravais lattice. The potential $W_p^s$ is assumed as a superposition of effective core potentials of the ions:

$$W_p^s = \sum_i^N V_i^{ion}, \tag{27}$$

where $V_i^{ion}$ is the ionic core potential at the site $i$ and $N$ is the number of ions in the solid. Since we are considering a semi-infinite solid, $W_p^s$ is periodic in each layer parallel to the $x$-$y$ plane, but not in the $z$ direction. The lattice constants in the $x$, $y$, and $z$ directions are $d_x$, $d_y$, and $d_z$, respectively. The $j$th ion in the $l$th layer has the coordinates $\mathbf{r}_{j,l} = (\mathbf{r}_{\parallel,j}, r_{\perp,l})$. Thus the periodic potential $W_p^s$ at the position $\mathbf{r}'$ can be written as

$$W_p^s(\mathbf{r}_\parallel', z') = \sum_l \sum_j V^{ion}(\mathbf{r}_\parallel' - \mathbf{r}_{\parallel,j}, z' - r_{\perp,l}). \tag{28}$$

Since $W_p^s$ is periodic in the $x$ and $y$ directions we can introduce [11,30] two-dimensional reciprocal vectors $\mathbf{g}_\parallel = 2\pi(n_x/d_x, n_y/d_y), n_x, n_y \in Z$, and write $W_p^s$ at the position $\mathbf{r}'$ as

$$W_p^s(\mathbf{r}_\parallel', z') = \sum_{\mathbf{g}_\parallel} \widetilde{W}_p^s(\mathbf{g}_\parallel, z') \exp(i \mathbf{g}_\parallel \cdot \mathbf{r}_\parallel'). \tag{29}$$

The two-dimensional $\mathbf{g}_\parallel$ Fourier transform $\widetilde{W}_p^s(\mathbf{g}_\parallel, z')$ is given by

$$\widetilde{W}_p^s(\mathbf{g}_\parallel, z') = \frac{1}{A_{uc}} \int_{uc} d^2 r_\parallel' W_p^s(\mathbf{r}_\parallel', z') \exp(-i \mathbf{g}_\parallel \cdot \mathbf{r}_\parallel'), \tag{30}$$

where $A_{uc}=d_x d_y$ is the surface of a unit cell in the $x$-$y$ layer and the integral in Eq. (30) runs over this unit cell. The expression $\langle \mathbf{q}|W_p^s|\mathbf{k}_i\rangle$, which enters Eq. (26), evaluates to

$$\begin{aligned}\langle \mathbf{q}|W_p^s|\mathbf{k}_i\rangle &= (2\pi)^{-3} f \sum_{\mathbf{g}_\parallel} \int d^3 r_p \exp(-i\mathbf{K}\cdot\mathbf{r}_p \\ &\quad + i\mathbf{g}_\parallel\cdot\mathbf{r}_{p,\parallel})\widetilde{W}_p^s(\mathbf{g}_\parallel, z_p) \\ &= (2\pi)^{-1} f \sum_{\mathbf{g}_\parallel} \delta^{(2)}(\mathbf{g}_\parallel - \mathbf{K}_\parallel)\int dz_p \widetilde{W}_p^s(\mathbf{g}_\parallel, z_p) \\ &\quad \times \exp(-iK_z z_p), \end{aligned} \tag{31}$$

where $\mathbf{K}:=\mathbf{q}-\mathbf{k}_i$ and $f=\exp(i\mathbf{q}\cdot\mathbf{r}_e)$. Thus the periodicity of the potential in the directions parallel to the surface leads to the Bragg condition $\mathbf{g}_\parallel=-\mathbf{K}_\parallel$. Upon substitution of Eqs. (28) and (30) into Eq. (31) and considering that $N=\Sigma_j \exp(-i\mathbf{g}_\parallel\cdot\mathbf{r}_{\parallel,j})$, Eq. (31) can be written in the form

$$\langle \mathbf{q}|W_p^s|\mathbf{k}_i\rangle = (2\pi)^{-3/2} f \widetilde{W}_p^s(\mathbf{K}). \tag{32}$$

The form factor $\widetilde{W}_p^s(\mathbf{K})$ derives to

$$\begin{aligned}\widetilde{W}_p^s(\mathbf{K}) &= \frac{N(2\pi)^2}{A_{uc}} \sum_{l,\mathbf{g}_\parallel} \delta^{(2)}(\mathbf{g}_\parallel - \mathbf{K}_\parallel) e^{-iK_z r_{\perp,l}} \int_{-\infty}^{\infty} d\rho_z \\ &\quad \times \int_{uc} d^2\rho_\parallel V^{ion}(\rho_\parallel, z_p)\exp[-i(\mathbf{g}_\parallel\cdot\boldsymbol{\rho}_\parallel + K_z\rho_z)], \end{aligned} \tag{33}$$

where $\boldsymbol{\rho}=\mathbf{r}_p-\mathbf{r}_j$. Within a model of nonoverlapping muffin-tin ionic potentials $V^{ion}$ the integration in Eq. (33) over the unit cell can be extended to the entire $x$-$y$ plane and we end up with the final expression

$$\widetilde{W}_p^s(\mathbf{K}) = \frac{N(2\pi)^2}{A_{uc}} \sum_l e^{-iK_z r_{\perp,l}} \sum_{\mathbf{g}_\parallel} \delta^{(2)}(\mathbf{g}_\parallel - \mathbf{K}_\parallel)\widetilde{V}^{ion}(\mathbf{K}). \tag{34}$$

In Eq. (34) $\widetilde{V}^{ion}(\mathbf{K})$ is the Fourier transform of $V^{ion}$. Here we use for the $V^{ion}$ screened Coulomb potential

$$V^{ion}(\mathbf{r}_p) = Z_{eff}/r_p \exp(-\lambda_{eff} r_p). \tag{35}$$

The effective parameters $Z_{eff}, \lambda_{eff}$ account for the screening of the pure ionic field due to the presence of the localized positive cores as well as delocalized electrons [30].

The initially bound electronic distribution is described by the effective one-body vector $|\chi_\mathbf{k}\rangle$. An expression for $|\chi_\mathbf{k}\rangle$ can be derived using the local-density functional method in which the ionic cores are considered as a constant positive ''background charge.'' Finding the many-body eigenstates of $H_e$ is then reduced to the iterative self-consistent solution of a one-body problem. Within the jellium model, the resultant effective one-particle potential is replaced by a step potential $V_0$ at $z=0$. Within the metal volume $V$ the conduction-band electrons are treated as free particles bound to the metal half space $z<0$ by a potential barrier

$$V_0 = \epsilon_F + W, \tag{36}$$

where $\epsilon_F$ is the Fermi energy and $W$ is the work function. The density of states is given by that of the free-electron gas (apart from a factor 2 that accounts for the electronic spin states) $\rho_j = V/(4\pi^3)$. Thus the jellium wave function can be expressed in terms of reflection and transmission coefficients

$$\langle \mathbf{r}_e|\chi_\mathbf{k}\rangle = \frac{1}{\sqrt{V}}\exp(i\mathbf{k}_\parallel\cdot\mathbf{r}_{e,\parallel})\times \begin{cases} e^{i\mathbf{k}_z z_e} + Re^{-i\mathbf{k}_z z_e}, & z<0 \\ Te^{-\gamma z_e}, & z>0. \end{cases} \tag{37}$$

The reflection and transmission coefficients $R$ and $T$ are given by

$$R = \frac{\mathbf{k}_z - i\gamma}{\mathbf{k}_z + i\gamma}, \quad T = \frac{2\mathbf{k}_z}{\mathbf{k}_z + i\gamma} \tag{38}$$

and $\gamma = \sqrt{2V_0 - \mathbf{k}_z^2}$.

As stated above, we consider cases of fast incoming and outgoing projectiles so that $|-Z_p/k_p| \ll 1$, i.e., the distortion of the projectile's motion due to $W_p^{vac}$ can be disregarded. The image-charge interaction of an electron with a semi-infinite metallic solid goes asymptotically to the classical limit $-1/4z$ [6]. Thus the eigenfunction of $H_f$ [Eq. (16)] at a given asymptotic energy $E_f$ is readily deduced as

$$\begin{aligned}\langle \mathbf{r}_e, \mathbf{r}_p|f\rangle &\approx \phi_f(\mathbf{r}_e, \mathbf{r}_p) \\ &= (2\pi)^{-3}\exp[i\mathbf{k}_p\cdot\mathbf{r}_p + i\mathbf{k}_e\cdot\mathbf{r}_e - i\varphi(\mathbf{r}_e)]. \end{aligned} \tag{39}$$

In Eq. (39) the term $\varphi(\mathbf{r}_e) = a\ln(2k_{e,z}z_e)$ is the phase modification of the asymptotically free electron motion due to its image charge where $k_{e,z}=\hat{\mathbf{z}}\cdot\mathbf{k}_e$ and the Sommerfeld parameter $a=-1/4k_{e,z}$ indicates the strength of this interaction. In the case $a\equiv 0$ we end up with the final-state being a product of two free-particle states. The final state energy is given by $E_f = k_e^2/2 + k_p^2/2m_p$.

As shown in Appendix A, the amplitude for the scattering of the projectile from the bulk $T_{p,s}^{sin}$ [Eq. (25)] can be derived analytically:

$$\begin{aligned}T_{p,s}^{sin} &= \sqrt{\frac{8}{\pi V}}\frac{Z_p Z_{eff} N}{A_{uc}} e^{-2\pi a/3}\Gamma(1+ia)\exp(ia\ln 2k_{e,z}) \\ &\quad \times \sum_{l,\mathbf{g}_\parallel} \delta^{(2)}(\mathbf{k}_\parallel - \mathbf{Q}_\parallel + \mathbf{g}_\parallel - \mathbf{k}_{e,\parallel})(\mathcal{L}_0 + \mathcal{L}_1 + \mathcal{L}_2), \end{aligned} \tag{40}$$

where the functions $\mathcal{L}_j, j=0,1,2$, are given by Eqs. (A21)–(A24). For the calculations of Eq. (40) the ionic-site potentials, given by Eq. (35), and the wave function (37) for the initially bound electron have been employed. We note here that in the course of the derivation of Eq. (40) a distinction had to be made between the transmission and reflection mode (with respect to the momentum of ejected electron). Equation (40) is valid for reflection mode. The expression of $T_{p,s}^{sin}$ under transmission conditions is easily derived following the procedure outlined in Appendix A (in this case and for higher incident energies we have to assume that the electron is ejected from jellium states of the surface opposite the projectile source as shown in Ref. [15]). In Eq. (40) the distortions of the motion of the ionized electron due to image-charge effects have been taken into account. For insu-

lating target or fast outgoing electrons these distortions can be switched off by the replacement $a \equiv 0$. The periodicity in the $x$-$y$ plane leads to the Lau-type condition expressed by the two-dimensional $\delta$ function in Eq. (40).

### B. Discussion of the single-scattering amplitude $T_{pe}^{sin}$

The amplitude $T_{pe}^{sin}$, as given by Eq. (19), describes the ionization process as a direct binary encounter of the projectile with the initially bound electron. As shown in Appendix B, its functional form is derived to

$$T_{pe}^{sin} = -iZ_p(2\pi V)^{-1/2}\delta^{(2)}(\mathbf{k}_\parallel - \mathbf{Q}_\parallel - \mathbf{k}_{e,\parallel})\frac{\Gamma(1+ia)}{Q^2}e^{-2\pi a/3} \times \exp[ia\ln(2k_{e,z})][(Q_z + k_{e,z} - k_z)^{-ia-1} + R(Q_z + k_{e,z} + k_z)^{-ia-1} - T(Q_z + k_{e,z} - i\gamma)^{-ia-1}]. \quad (41)$$

The free motion of the bound electron in the $x$-$y$ planes results in the two-dimensional $\delta$ function in Eq. (41). As in the case of ionization of atomic and molecular systems, the cross section decreases rapidly (proportionally to $1/Q^4$) with increasing momentum transfer. This is a direct consequence of the assumption that the perturbation leading to the electron ejection possesses the Coulombnic functional form (A1).

## IV. MULTIPLY DIFFERENTIAL CROSS SECTIONS

The multiply differential cross section for the simultaneous detection of the escaping particles with momenta $\mathbf{k}_e, \mathbf{k}_p$ following charged-particle impact is [31]

$$\sigma(\mathbf{k}_i, \mathbf{k}) = (2\pi)^4 \frac{1}{v_i}\sum\!\!\!\!\!\!\int |T|^2 \delta(E_f - E_i)\delta^{(3)} \times (\mathbf{P}_f - \mathbf{P}_i) d^3\mathbf{k}_e d^3\mathbf{k}_p d^3\mathbf{k}_{core}, \quad (42)$$

where $v_i = |\mathbf{k}_i|/m_p$, $\mathbf{P}_f, \mathbf{P}_i$ are the total linear momenta in the final and initial channels, and $\mathbf{k}_{core}$ is the momentum absorbed by the solid. Thus the $\delta$ functions in Eq. (42) indicate the total momentum and the energy-conservation laws. In Eq. (42) the symbol $\sum\!\!\!\!\!\!\int$ signifies summation or integration over all nonresolved final- and initial-state quantum numbers. Assuming a ''frozen-core'' approximation, due to which all degrees of freedom of the system except for those of the projectile and the active electron remain unchanged during the ionization process, the total linear momentum in the initial state reduces to $\mathbf{P}_i = \mathbf{k}_i + \mathbf{k}$. The total linear momentum in the final channel is $\mathbf{P}_f = \mathbf{k}_p + \mathbf{k}_e + \mathbf{k}_{core}$. In addition, we deduce $E_i = k_i^2/2m_p - E_{\mathbf{k}} - W$ and $E_f = k_p^2/2m_p + k_e^2/2$. Within these approximations Eq. (42) simplifies to

$$\sigma(\mathbf{k}_i, \mathbf{k}) = (2\pi)^4 \frac{1}{v_i}|T|^2 \delta(E_f - E_i) d^3\mathbf{k}_e d^3\mathbf{k}_p. \quad (43)$$

Usually [7,16,23,25,26], the coincidence rate is measured as a function of the energies $E_e, E_p$ and the solid angles $\Omega_e, \Omega_p$ of the emitted electron and scattered projectile, respectively. In this case Eq. (43) reads

$$\frac{d\sigma(\mathbf{k}_i, \mathbf{k})}{d^2\Omega_e dE_e d^2\Omega_p dE_p} = (2\pi)^4 \frac{k_p k_e}{v_i}|T|^2 (E_f - E_i). \quad (44)$$

### Integration over the conduction band

Equation (44) yields, for given values of $\mathbf{k}_i, \mathbf{k}_e, \mathbf{k}_p$, the ionization probability of an initial solid state defined by $\mathbf{k}$. At present, coincident experiments do not resolve these states. Thus an integration over $\mathbf{k}$ is necessary:

$$\frac{d\sigma(\mathbf{k}_i)}{d^2\Omega_e dE_e d^2\Omega_p dE_p} = \int d^3\mathbf{k}\rho(\mathbf{k})F(\mathbf{k}, T) \times \frac{d\sigma(\mathbf{k}_i, \mathbf{k})}{d^2\Omega_e dE_e d^2\Omega_p dE_p}, \quad (45)$$

where $\rho(\mathbf{k})$ is the density of states at the temperature $T$ and $F(\mathbf{k}, T)$ is the Fermi distribution. In the jellium model [$\rho(\mathbf{k}) = \rho_j = V/4\pi^3$] and at $T = 0$, Eq. (45) simplifies to

$$\frac{d\sigma(\mathbf{k}_i)}{d^2\Omega_e dE_e d^2\Omega_p dE_p} = \rho_j \int_{k \le k_F} d^3\mathbf{k} \frac{d\sigma(\mathbf{k}_i, \mathbf{k})}{d^2\Omega_e dE_e d^2\Omega_p dE_p}. \quad (46)$$

For the scattering amplitudes, given by Eqs. (19) and (25), the integration over the conduction band can be carried out analytically.

## V. NUMERICAL RESULTS AND IONIZATION MECHANISMS

The procedure developed above is applicable to scattering events in the transmission and reflection mode. The explicit formulas (40) and (41) for the scattering amplitudes are valid for the case of the reflection mode. In order to apply this method to a particular target the parameters for the projectile-bulk scattering potential (35) have to be specified as well as the number of atoms $N$ in the semi-infinite solid. The effective parameters $\lambda_{eff}$ and $Z_{eff}$, which account for the screening of the projectile-ion interactions due to localized and delocalized electronic states, can be determined from the Thomas-Fermi model [32,30]

$$\lambda_{eff} = \sqrt{\frac{3k_F}{\pi}}. \quad (47)$$

In this work we present numerical calculations for an aluminum surface. In this case we obtain $\lambda_{eff} = 0.886$, which is consistent with the assumption of nonoverlapping muffin-tin ionic potentials that has been made in Eqs. (27) and (33). For $Z_{eff}$ we assume full screening by localized electrons, which leads to $Z_{eff} = 1$. The proportionality of the second-order scattering amplitude (40) to the number of scattering centers $N$ implies a divergent cross section for an infinite surface. This same problem is encountered in the scattering of thermic neutrons from crystals, in LEED processes [11], as well as in the treatment of transfer processes of electronic states of a surface into the spectrum of an ionic beam scattered from this surface [30]. The origin of this difficulty is the neglect of crystal-damping effects on propagating beams,

e.g., in Eq. (26) the incoming plane wave $|\mathbf{k}_i\rangle$ is elastically scattered into $|\mathbf{q}\rangle$ under the coherent action of $N$ cores per plane. In LEED reactions this problem is circumvented by estimating the number of cores in the solid illuminated by the incoming beam and relating them to $N$ [11]. In our case we adopt a similar procedure by relating $N$ to the number of ionic cores $N_{cores}$ in a cylinder of radius $\overline{\lambda}$ and height $\overline{\lambda}$, where $\overline{\lambda}$ refers to the mean free path of the impinging electron beam. This is reasonable since, as remarked above, the divergent $N$ dependence of Eq. (40) is traced back to the projectile-bulk elastic scattering. We remark here that for a specific experimental geometry the scattering amplitude (40) does not depend on the parameters $N$ and $Z_{eff}$ in a dynamical way, i.e., these parameters affect only the magnitude of this amplitude. Nevertheless, in cases where the amplitudes (40) and (19) are of the same order, the interference pattern of these amplitudes can sensitively depend on the product $NZ_{eff}$.

### Ionization mechanisms

For electron-impact ionization of an aluminum surface we calculated the cross section (46) by performing a numerical summation over $\mathbf{g}_{\|}$ and $l$. As stated above, the present theory is applicable at moderate energies of the incoming and outgoing particles (only the classical $1/4z$ image-charge electron-surface interaction is taken into account). Classically, the electron emission in the reflection mode is prohibited in a one-step mechanism as described by Eq. (19). Hence, for $k_e, k_p \gg k_F$, where classical arguments are applicable, the contribution to the cross section of Eq. (19) is negligibly small compared to that of the second-order amplitude (40).

The possible collisional ionization mechanisms described within this model are schematically depicted in Figs. 1(a)–1(d). In all cases it is assumed that the velocity of the impinging and emitted particles are large with respect to the initial momentum distribution of the electronic solid state. In order to get some insight into the influence of these mechanisms on the spectra of the electrons we analyze Figs. 1(a)–1(d) within a simple classical model in which we assume the target electron to be stationary and the bulk potential to act as a structureless reflection mirror in the $x$-$y$ plane (due to the Lau condition parallel to the surface). Subsequently we look at the prediction of this simplified picture in light of the full quantum-mechanical calculations. Classically, the case shown in Fig. 1(a) means that the projectile is directly scattered into the vacuum after an inelastic binary encounter with the delocalized electron and escape with momentum $\mathbf{k}_p$. This electron is then elastically reflected from the bulk and emerges into the vacuum with momentum $\mathbf{k}_e$. Within the full quantum-mechanical model, the latter interaction is facilitated by the initial-state binding. Within the classical model assumed above, this mechanism leads to a peak structure in the angular distribution of the continuum particles at $\theta_p = \theta_i - \arctan k_p/k_e, \theta_e = \pi - \theta_i - \arctan k_p/k_e, \phi_e - \phi_p = 0,$ as can be deduced from simple kinematic consideration of Fig. 1(a). The appearance of the peak at the classically predicted position is endorsed by the full quantum calculations as demonstrated in Fig. 2(a). Since the projectile suffers relatively small momentum loss, the magnitude of the cross section is quite sizable. The classical model predicts a $\delta$-function distribution at the position marked by the arrow in Fig. 2(a). The broadness of the peak [Fig. 2(a)] predicted by the model presented in the previous sections is related to the electronic initial momentum distribution.

The classical mechanism displayed in Fig. 1(b) corresponds to the quantum-mechanical picture where the delocalized electronic state is directly transferred into a vacuum state following an inelastic collision with the projectile. As in a LEED process, the scattered projectile is then refracted from the bulk potential (35). This process is described by the amplitude (40). In contrast, the single-scattering amplitude (41) does not contain any projectile scattering from the bulk. Our simplified classical model yields for the mechanism displayed in Fig. 1(b) a $\delta$-function structure in the angular distribution of the emerging particles at $\theta_p = \pi - \theta_i - \arctan k_e/k_p, \theta_e = \theta_i - \arctan k_p/k_e, \phi_e - \phi_p = 0$. The occurrence of this peak is nicely confirmed by the full quantum-mechanical model [Fig. 2(b)] with the initial momentum distribution of the secondary electron being reflected in the shape of the peak in Fig. 2(b). Due to the much larger momentum transfer, the cross section depicted in Fig. 2(b) is markedly smaller than that of Fig. 2(a).

In the classical case sketched in Fig. 1(c) both the electron and the projectile are reflected from the bulk potential after a binary (isolated) encounter. Quantum mechanically, this process is facilitated by the scattering amplitude (40) only. The classical kinematic conditions, under which this reaction shows up in the angular distribution, are given by $\theta_p = \arctan k_e/k_p + \pi - \theta_i$, $\theta_e = \arctan k_p/k_e - \pi + \theta_i$, $\phi_e - \phi_p = \pm\pi$. A comparison of the quantum model with those predictions is shown in Fig. 2(c). Since the electron, whose angular distribution is shown in Fig. 2(c), is much faster than the cases of Figs. 2(a) and 2(b), the peak at $\theta_p \approx 50.5°$ is much sharper. This is due to the fact that the initial momentum distribution of the secondary electron is almost negligible with respect to $k_p$, i.e., during the interaction time the initially bound electron appears to be stationary from the viewpoint of the fast scattered electron.

The last classical kinematics discussed here is that of Fig. 1(d), where the projectile is mirror reflected from the bulk. Subsequently, the electron and the projectile are directly transferred into vacuum levels following an isolated binary scattering. Within the model discussed in the previous sections, this process is described by the scattering amplitude (40). From the simple classical picture it is anticipated that the cross section reveals a $\delta$-function structure at $\theta_e = \arctan k_p/k_e + \pi - \theta_i$, $\theta_p = \arctan k_e/k_p - \pi + \theta_i$, $\phi_e = 0, \phi_p = \pi$. This is confirmed by the quantum model [Fig. 2(c)]; however, the peaks are quite shallow and clearly shifted from the classically predicted position. This is a consequence of the high momentum transfer to the crystal and the relatively low velocity of the escaping particles as compared to the Fermi velocity. The same process depicted in Fig. 1(c) has been proposed previously in Refs. [25–27] to describe the observed spectra of two electrons simultaneously emitted following electron impact upon a clean tungsten surface. We repeated the calculations shown in Fig. 2 for a tungsten surface. Structures similar to those in Fig. 2 (even more pronounced) have been observed. The application of the present model to the experiments presented in Refs. [25–27], how-

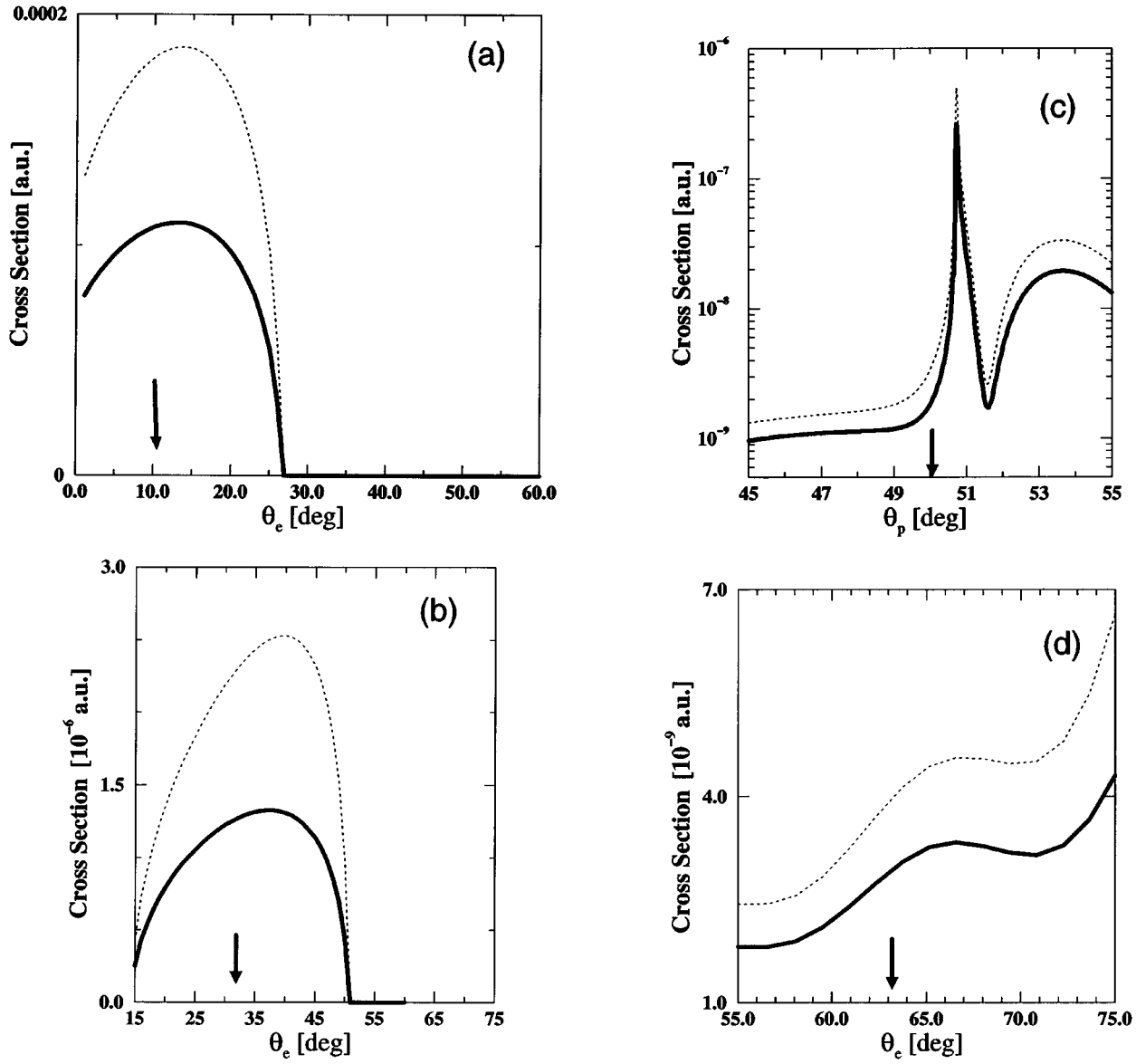


FIG. 2. Angular distributions of electrons ejected from a semi-infinite aluminum solid upon electron impact. In cases (a)–(c) the impact energy is chosen as $E_i = 518$ eV with respect to the vacuum threshold. The ejected electron escapes with an energy $E_e = 60$ eV, whereas the scattered one emerges with an energy $E_p = 453$ eV. The vectors $\mathbf{k}_i$, $\mathbf{k}_e$, and $\mathbf{k}_p$ are chosen to lie in the same $(x,z)$ plane. (a) The scattering geometry is $\theta_i = 100°, \theta_p = 80°$, and $\varphi_i = \varphi_p = \varphi_e = 0°$. The cross section is scanned as function of $\theta_e$. (b) Same as in (a), but $\theta_p = 60°$. (c) Same as in (a), but $\theta_i = 150°$, $\theta_e = 40°$, $\varphi_i = \varphi_p = 0°$, and $\varphi_e = 180°$. (d) We choose $E_i = 418$ eV, $E_p = 302$ eV, and $E_e = 110$ eV. In addition, $\theta_i = 178°$, $\theta_p = 29°$, $\varphi_i = \varphi_e = 0°$, and $\varphi_p = 180°$. The solid curves correspond to an antisymmetrized product of the final-state wave function (39) with image-charge distortions of the escaping particles being neglected, whereas these distortions are taken into account in the calculations shown by the dotted curves. In all figures the arrows indicate the positions of the peaks as predicted by the kinematics of the processes depicted in Figs. 1(a)–1(d) (see the text for details).

ever, is questionable since these experiments have been conducted at quite low energies, whereas the present model and the kinematic arguments are valid only at momenta of the vacuum particles that are much larger than the Fermi momentum. At higher energies, the influence of this mechanism on the cross section is clearly seen in Fig. 2(c).

Generally, the processes sketched in Figs. 1(a) and 1(b) are most likely to dominate in the grazing incidence direction. This conclusion relies upon the fact that, in grazing incidence, the traveling distance of the projectile before reaching the bulk is much larger than in the case of normal incidence geometry. In fact, further numerical investigations [33] using an Al surface show that the dominant contribution to the $(e,2e)$ cross section as reported in Ref. [23] is due to the mechanism depicted in Fig. 1(a).

As evident from Figs. 2(a)–2(d), the final-state image-charge interaction enhances the coincidence rate. This is due to the fact that a scattering from the ionic core is essential in the reflection geometry. This scattering can occur, however, via a final-state image-charge interaction with the solid. All calculations shown in Figs. 2(a)–2(d) have been performed using a coherent sum of the transition amplitudes (40) and (41). The sum over $\mathbf{g}_\parallel, l$ is rapidly convergent. In fact, it turned out that by far the significant contribution to the scat-

tering amplitudes is provided by scattering from the first and, in some cases, from the second $l$ layers.

## VI. CONCLUSION

In this work a theoretical description of the scattering of fast (with respect to the Fermi velocity) charge particles from a clean metallic semi-infinite solid has been presented. For semi-infinite aluminum solid, calculations of the multiple differential cross section have been performed using a jellium initial-state wave function of the surface. A final-state electron-surface image-charge interaction has been included in its asymptotic form. LEED scattering of the incident electron from the periodic bulk potential has also been included. From a kinematic analysis four different ionization mechanisms have been deduced and confirmed by the full dynamical model.

## ACKNOWLEDGMENTS

We would like to thank M. Vos, E. Weigold, S. Buckman, U. Thumm, and A. Kheifets for helpful suggestions and comments. Support by the Australian National University is gratefully acknowledged.

## APPENDIX A: ANALYTICAL EVALUATION OF $T_{p,s}^{sin}$

To derive an expression for the scattering amplitude (25) we perform in this appendix the integrals involved in Eqs. (25) and (26). The initially undisturbed electronic solid state is described by the wave function given by Eq. (37). To avoid difficulties arising from the infinite range of Coulomb interactions we introduce the cutoff potential

$$W_{pe}=\lim_{\eta_1\to 0^+}\frac{-Z_p\exp(-\eta_1|\mathbf{r}_e-\mathbf{r}_p|)}{|\mathbf{r}_e-\mathbf{r}_p|}. \tag{A1}$$

Thus expression (26) can be written as

$$F=-Z_p\lim_{\eta_1,\eta_2\to 0^+}(2\pi)^{-3}\int d^3\mathbf{q}\exp[i(\mathbf{q}-\mathbf{k}_p)\cdot\mathbf{r}_e]\widetilde{W}_{pe}\times(\mathbf{k}_p-\mathbf{q},\eta_1)\frac{1}{\mathbf{K}_-^2-\mathbf{q}^2-i\eta_2}\widetilde{W}_p^s(\mathbf{q}-\mathbf{k}_i). \tag{A2}$$

Upon substituting the form factor $\widetilde{W}_p^s(\mathbf{q}-\mathbf{k}_i)$ [Eq. (34)] into Eq. (A2) we obtain

$$F=\frac{-2(2\pi)^{-3/2}Z_pN}{A_{uc}}\lim_{\eta_1,\eta_2\to 0^+}\sum_{l,\mathbf{g}_\parallel}\int d^3\mathbf{q}\delta^{(2)}(\mathbf{g}_\parallel-\mathbf{K}_\parallel)\times\exp[i(\mathbf{q}-\mathbf{k}_p)\cdot\mathbf{r}_e]\frac{\exp(-iK_zr_{\perp,l})\widetilde{V}^{ion}(\mathbf{K})}{(|\mathbf{k}_p-\mathbf{q}|^2+\eta_1^2)(\mathbf{K}_-^2-\mathbf{q}^2-i\eta_2)}. \tag{A3}$$

Changing variables from $\mathbf{q}$ to $\mathbf{K}$ the expression (25) for $T_{p,s}^{sin}$ simplifies to

$$T_{p,s}^{sin}=\int d^3\mathbf{K}\mathcal{F}(\mathbf{K})I(\mathbf{K}), \tag{A4}$$

where

$$\mathcal{F}:=\frac{-2(2\pi)^{-3/2}Z_pN}{A_{uc}}\lim_{\eta_1,\eta_2\to 0^+}\sum_{l,\mathbf{g}_\parallel}\delta^{(2)}(\mathbf{g}_\parallel-\mathbf{K}_\parallel)\times\frac{\exp(-iK_zr_{\perp,l})\widetilde{V}^{ion}(\mathbf{K})}{(|\mathbf{Q}-\mathbf{K}|^2+\eta_1^2)[\mathbf{K}_-^2-(\mathbf{K}+\mathbf{k}_i)^2-i\eta_2]}. \tag{A5}$$

In Eq. (A5) the momentum transfer vector $\mathbf{Q}:=\mathbf{k}_p-\mathbf{k}_i$ has been defined. Using Eq. (39) for the final state, the function $I(\mathbf{K})$, which occurs in Eq. (A4), is readily deduced to

$$I(\mathbf{K})=(2\pi)^{-3/2}\int d^3\mathbf{r}_e\exp[-i(\mathbf{Q}+\mathbf{k}_e-\mathbf{K})\cdot\mathbf{r}_e+i\varphi(\mathbf{r}_e)]\chi_{\mathbf{k}}(\mathbf{r}_e). \tag{A6}$$

Using the integral representation

$$z^{-a}=\frac{1}{\Gamma(a)}\int_0^\infty dt\exp(-zt)t^{a-1},\quad \mathrm{Re}(a)>0,\quad \mathrm{Re}(z)>0, \tag{A7}$$

the logarithmic phase in the integral (A6) can be rewritten as

$$\exp(i\varphi)=\lim_{\eta_3\to 0^+}\frac{1}{\Gamma(\alpha)}\int_0^\infty dt\exp(-\boldsymbol{\xi}\cdot\mathbf{r}_e)t^{\alpha-1}, \tag{A8}$$

where $\alpha=-ia+\eta_3$ [we recall that $a=-1/(4k_{e,z})$] and $\boldsymbol{\xi}:=2k_{e,z}t\hat{\mathbf{z}}$. Thus the integral $I(\mathbf{K})$ evaluates to

$$I(\mathbf{K})=\lim_{\eta_3\to 0^+}\frac{1}{\Gamma(\alpha)}\int_0^\infty dtt^{\alpha-1}\widetilde{\chi}_{\mathbf{k}}(\mathbf{\Lambda},t), \tag{A9}$$

where

$$\widetilde{\chi}_{\mathbf{k}}(\mathbf{\Lambda},t)=i\sqrt{\frac{2\pi}{V}}\delta^{(2)}(\mathbf{k}_\parallel-\mathbf{\Lambda}_\parallel)\left(\frac{1}{\Lambda_z-k_z}+\frac{R}{\Lambda_z+k_z}-\frac{T}{\Lambda_z-i\gamma}\right). \tag{A10}$$

The vector $\mathbf{\Lambda}$ is given by $\mathbf{\Lambda}:=\mathbf{Q}-\mathbf{K}+\mathbf{k}_e-i\xi$. Using the screened Coulomb potentials, given by Eq. (35), for the muffin-tin ion potentials $V^{ion}$, Eq. (A4) reduces to

$$T_{p,s}^{sin}=\lim_{\eta_1,\eta_2,\eta_3\to 0^+}\frac{-NZ_pZ_{eff}}{\pi^2A_{uc}\Gamma(\alpha)}\int_0^\infty dtt^{\alpha-1}\sum_{l,\mathbf{g}_\parallel}II(t,l,\mathbf{g}_\parallel), \tag{A11}$$

where

$$II(t,l,\mathbf{g}_\parallel):=\int_{-\infty}^\infty dK_zY(K_z,t,l,\mathbf{g}_\parallel) \tag{A12}$$

and

$$Y(K_z,t,l,\mathbf{g}_\parallel)=\exp(-iK_z r_{\perp,l})\tilde{\chi}_{\mathbf{k}}(\mathbf{\Lambda},\mathbf{K}_\parallel=\mathbf{g}_\parallel)[|\mathbf{Q}_\parallel-\mathbf{g}_\parallel|^2+(Q_z-K_z)^2+\eta_1^2]^{-1}[\mathbf{K}_-^2-|\mathbf{k}_{i,\parallel}+\mathbf{g}_\parallel|^2-(k_{i,z}+K_z)^2-i\eta_2]^{-1}[\mathbf{g}_\parallel^2+K_z^2+\lambda_{eff}^2]^{-1}. \tag{A13}$$

An expression for the integral (A12) is obtained by converting $K_z$ to a complex variable and considering the improper contour integral

$$II(t,l,\mathbf{g}_\parallel)=\lim_{\rho\to\infty}\oint_{\partial G_\rho} dK_z Y(K_z,t,l,\mathbf{g}_\parallel). \tag{A14}$$

since $r_{\perp,l}<0$ ($r_{\perp,0}=-d_z/2$) we choose the domain $G$ as the upper half of the complex plane, i.e., $G=\{K_z|\mathrm{Im}(K_z)>0,|K_z|<\rho\}$. The function $Y(K_z)$ is meromorphic in $G$, i.e., it possesses only isolated singularities and thus can be evaluated via calculus of residues. The poles of $Y(K_z)$ in $G$ depend on the sign of $k_{e,z}$ and hence on the geometry in which the experiment is performed. In a transmission experiment $k_{e,z}$ is negative, whereas $k_{e,z}>0$ in reflection geometry. Here we perform the calculations in reflection geometry; similar considerations apply to transmission mode. The poles of $Y(K_z)$ in $G$ are determined to be

$$z_0=Q_z+i[|\mathbf{Q}_\parallel-\mathbf{g}_\parallel|^2+\eta_1^2]^{1/2}, \tag{A15}$$

$$z_1=\begin{cases}-k_{i,z}-[\mathbf{K}_-^2-|\mathbf{k}_{i,\parallel}+\mathbf{g}_\parallel|^2-i\eta_2]^{1/2} & \text{if } \mathbf{K}_-^2>|\mathbf{k}_{i,\parallel}+\mathbf{g}_\parallel|^2\\ -k_{i,z}+[\mathbf{K}_-^2-|\mathbf{k}_{i,\parallel}+\mathbf{g}_\parallel|^2-i\eta_2]^{1/2} & \text{if } \mathbf{K}_-^2<|\mathbf{k}_{i,\parallel}+\mathbf{g}_\parallel|^2,\end{cases} \tag{A16}$$

$$z_2=i(\mathbf{g}_\parallel^2+\lambda_{eff}^2)^{1/2}. \tag{A17}$$

Thus the integral (A14) can be expressed as

$$II(t,l,\mathbf{g}_\parallel)=2\pi i\sum_{\nu=0}^{2}\mathrm{Res}_{z_\nu}Y(K_z,t,l,\mathbf{g}_\parallel). \tag{A18}$$

Inserting Eq. (A18) into Eq. (A4), the remaining $t$ integral can be carried out analytically by using the integral representation of the $\beta$ function [34]

$$\int_0^\infty t^{\mu-1}(1+\beta t)^{-\nu}dt=\beta^{-\mu}B(\mu,\nu-\mu),$$

$$|\arg\beta|<\pi,\quad \mathrm{Re}(\nu)>\mathrm{Re}(\mu)>0. \tag{A19}$$

Furthermore, using the relation $B(x,y)=\Gamma(x)\Gamma(y)/\Gamma(x+y)$, we end up with the expression

$$T_{p,s}^{sin}=\sqrt{\frac{8}{\pi V}}\frac{Z_pZ_{eff}N}{A_{uc}}e^{-2\pi a/3}\Gamma(1+ia)\exp(ia\ln 2k_{e,z})\times\sum_{l,\mathbf{g}_\parallel}\delta^{(2)}(\mathbf{k}_\parallel-\mathbf{Q}_\parallel+\mathbf{g}_\parallel-\mathbf{k}_{e,\parallel})(\mathcal{L}_0+\mathcal{L}_1+\mathcal{L}_2), \tag{A20}$$

where

$$\mathcal{L}_0=\exp(-iz_0r_{\perp,l})\mathcal{B}_0[2i|\mathbf{Q}_\parallel-\mathbf{g}_\parallel|]^{-1}[\mathbf{K}_-^2-|\mathbf{k}_{i,\parallel}+\mathbf{g}_\parallel|^2-(k_{i,z}+z_0)^2]^{-1}[\mathbf{g}_\parallel^2+z_0^2+\lambda_{eff}^2]^{-1}. \tag{A21}$$

In the case $\mathbf{K}_-^2>|\mathbf{k}_{i,\parallel}+\mathbf{g}_\parallel|^2$ we obtain for $\mathcal{L}_1$

$$\mathcal{L}_1=\frac{-1}{2}\exp(-iz_1r_{\perp,l})\mathcal{B}_1[|\mathbf{Q}_\parallel-\mathbf{g}_\parallel|^2+(Q_z-z_1)^2]^{-1}\times[\mathbf{K}_-^2-|\mathbf{k}_{i,\parallel}+\mathbf{g}_\parallel|^2]^{-1/2}[\mathbf{g}_\parallel^2+z_1^2+\lambda_{eff}^2]^{-1}, \tag{A22}$$

whereas if $\mathbf{K}_-^2<|\mathbf{k}_{i,\parallel}+\mathbf{g}_\parallel|^2$ the following relation is valid:

$$\mathcal{L}_1=\frac{-i}{2}\exp(-iz_1r_{\perp,l})\mathcal{B}_1[|\mathbf{Q}_\parallel-\mathbf{g}_\parallel|^2+(Q_z-z_1)^2]^{-1}\times[-\mathbf{K}_-^2+|\mathbf{k}_{i,\parallel}+\mathbf{g}_\parallel|^2]^{-1/2}[\mathbf{g}_\parallel^2+z_1^2+\lambda_{eff}^2]^{-1}. \tag{A23}$$

Finally, the expression for $\mathcal{L}_2$ reads

$$\mathcal{L}_2=\frac{-i}{2\sqrt{\mathbf{g}_\parallel^2+\lambda_{eff}^2}}\exp(-iz_2r_{\perp,l})\mathcal{B}_2[|\mathbf{Q}_\parallel-\mathbf{g}_\parallel|^2+(Q_z-z_2)^2]^{-1}[\mathbf{K}_-^2-|\mathbf{k}_{i,\parallel}+\mathbf{g}_\parallel|^2-(k_{i,z}+z_2)^2]^{-1}. \tag{A24}$$

The functions $\mathcal{B}_j, j=0,1,2$ have been defined as

$$\mathcal{B}_j:=(b_j-k_z)^{-ia-1}+R(b_j+k_z)^{-ia-1}-T(b_j-i\gamma)^{-ia-1}, \tag{A25}$$

where $b_j:=\mathbf{Q}_z-z_j+k_{e,z}$.

## APPENDIX B: EVALUATION OF THE SINGLE-SCATTERING AMPLITUDE $T_{pe}^{sin}$

In this appendix we carry out the integrals involved in Eq. (19). Making use of Eqs. (A1), (39), and (37), Eq. (19) reads

$$T_{pe}^{sin}=-Z_p(2\pi)^{-9/2}\lim_{\eta_1\to 0^+}\int d\mathbf{r}_p d\mathbf{r}_e\exp\{-i[\mathbf{Q}\cdot\mathbf{r}_p+\mathbf{k}_e\cdot\mathbf{r}_e-\varphi(\mathbf{r}_e)]\}\frac{\exp(-\eta_1|\mathbf{r}_e-\mathbf{r}_p|)}{|\mathbf{r}_e-\mathbf{r}_p|}\chi_{\mathbf{k}}(\mathbf{r}_e). \tag{B1}$$

Upon replacing the logarithmic phase in Eq. (B1) by its integral representation, given by Eq. (A8), and performing the integral over the projectile coordinates, Eq. (B1) simplifies to

$$T_{pe}^{sin}=\frac{-Z_p}{2\pi^2}\lim_{\eta_3,\eta_1\to 0^+}\frac{1}{\Gamma(\alpha)[Q^2+\eta_1^2]}\int_0^\infty dt t^{\alpha-1}J(t), \tag{B2}$$

where

$$J(t)=(2\pi)^{-3/2}\int d\mathbf{r}_e\exp[-i(\mathbf{Q}+\mathbf{k}_e-i\boldsymbol{\xi})\cdot\mathbf{r}_e]\chi_{\mathbf{k}}(\mathbf{r}_e)=\tilde{\chi}_{\mathbf{k}}(\overline{\mathbf{\Lambda}},t). \tag{B3}$$

In Eq. (B3) we introduced the complex vector $\overline{\mathbf{\Lambda}}:=\mathbf{Q}+\mathbf{k}_e-i\xi$. Analogously to Eq. (A10), the Fourier transform $J(t)$ evaluates to

$$J(t)=i\sqrt{\frac{2\pi}{V}}\delta^{(2)}(\mathbf{k}_\parallel-\overline{\mathbf{\Lambda}}_\parallel)\left(\frac{1}{\overline{\Lambda}_z-k_z}+\frac{R}{\overline{\Lambda}_z+k_z}-\frac{T}{\overline{\Lambda}_z-i\gamma}\right). \tag{B4}$$

Now inserting Eq. (B4) into Eq. (B2), the remaining one-dimensional integral can be algebraically transformed to the $\beta$-function integral representation, given by Eq. (A19):

$$T_{pe}^{sin}=-iZ_p(2\pi V)^{-1/2}\delta^{(2)}(\mathbf{k}_\parallel-\overline{\mathbf{\Lambda}}_\parallel)\times\lim_{\eta_3,\eta_1\to 0^+}\frac{1}{\Gamma(\alpha)[Q^2+\eta_1^2]}(J_1+RJ_2-TJ_3). \tag{B5}$$

The functions $J_i$ are given by

$$J_i=\overline{b_i}^{-1}\int_0^\infty dt t^{\alpha-1}\left(1+\frac{-i2k_{e,z}}{\overline{b_i}}t\right)^{-1},\quad i=1,2,3, \tag{B6}$$

where $\overline{b_1}=Q_z+k_{e,z}-k_z$, $\overline{b_2}=Q_z+k_{e,z}+k_z$, and $\overline{b_3}=Q_z+k_{e,z}-i\gamma$. Making use of Eq. (A19) and after some elementary algebra we end up with the final expression

$$T_{pe}^{sin}=-iZ_p(2\pi V)^{-1/2}\delta^{(2)}(\mathbf{k}_\parallel-\overline{\mathbf{\Lambda}}_\parallel)\frac{\Gamma(1+ia)}{Q^2}e^{-2\pi a/3}\times\exp[ia\ln(2k_{e,z})][\overline{b_1}^{ia-1}+R\overline{b_2}^{ia-1}-T\overline{b_3}^{ia-1}]. \tag{B7}$$


[1] I. E. McCarthy and E. Weigold, Rep. Prog. Phys. **54**, 789 (1991).
[2] H. Ehrhardt, K. Jung, G. Knoth, and P. Schlemmer, Z. Phys. D **1**, 3 (1986).
[3] F. W. Byron, Jr., and C. J. Joachain, Phys. Rep. **179**, 211 (1989).
[4] C. T. Whelan, R. J. Allan, J. Rasch, H. R. J. Walters, X. Zhang, J. Röder, K. Jung, and H. Ehrhardt, Phys. Rev. A **50**, 4394 (1994).
[5] J. Berakdar, J. Röder, J. S. Briggs, and H. Ehrhardt, J. Phys. B **29**, 1767 (1996).
[6] P. J. Jenning, R. O. Jones, and M. Weinert, Phys. Rev. B **37**, 6113 (1988).
[7] R. Camilloni, A. Giardini Guidoni, R. Tiribelli, and G. Stefani, Phys. Rev. Lett. **29**, 618 (1972).
[8] H. Ehrhardt, M. Schulz, T. Tekaat, and K. Willmann, Phys. Rev. Lett. **22**, 89 (1969).
[9] U. Amaldi, A. Egioli, R. Marconero, and G. Pizella, Rev. Sci. Instrum. **40**, 1001 (1969).
[10] C. B. Duke, in *Advances in Chemical Physics*, edited by I. Prigogine and S. A. Rice (Wiley, New York, 1974), Vol. 27.
[11] J. B. Pendry, *Low Energy Electron Diffraction* (Academic, London, 1974).
[12] C. B. Duke and C. E. Laramore, Phys. Rev. B **2**, 4765 (1970).
[13] E. R. Jones, J. I. McKinney, and M. B. Webb, Phys. Rev. **151**, 476 (1966).
[14] H. Bethe, Ann. Phys. (Leipzig) **5**, 325 (1930).
[15] I. E. McCarthy and E. Weigold, Contemp. Phys. **35**, 377 (1994).
[16] M. Vos and I. E. McCarthy, Rev. Mod. Phys. **67**, 713 (1995).
[17] A. D'Andrea and R. Del Sole, Surf. Sci. **71**, 306 (1978).
[18] V. G. Levin, N. G. Neudatchin, and Yu. F. Smirnov, Phys. Status Solidi B **29**, 618 (1972).
[19] L. J. Allen, I. E. McCarthy, V. W. Maslen, and C. J. Rossouw, Aust. J. Phys. **43**, 453 (1990).
[20] X. Guo, S. Canney, A. S. Kheifets, M. Vos, Z. Fang, S. Utteridge, I. E. McCarthy, and E. Weigold, Phys. Rev. B **54**, 17 943 (1996).
[21] A. S. Kheifets and Y. Q. Cai, J. Phys., Condens. Matter. **7**, 1821 (1995).
[22] A. S. Kheifets and M. Vos, J. Phys., Condens. Matter. **7**, 3895 (1995).
[23] S. Iacobucci, L. Marassi, R. Camilloni, S. Nannarone, and G. Stefani, Phys. Rev. B **51**, R10 252 (1995).
[24] G. Stefani, L. Avaldi, and R. Camilloni, J. Phys. (Paris) IV, Colloq. **6**, C6-1 (1993).
[25] J. Kirschner, O. M. Artamonov, and A. N. Terekhov, Phys. Rev. Lett. **69**, 1711 (1992).
[26] O. M. Artamonov, S. N. Samarin, and J. Kirschner, Phys. Rev. B **51**, 2491 (1995).
[27] J. Kirschner, O. M. Artamonov, and S. N. Samarin, Phys. Rev. Lett. **75**, 2424 (1995).
[28] H. Gollisch, G. Meinert, Xiao Yi, and R. Feder, Solid State Commun. (to be published).
[29] M. A. Van Hove, W. H. Weinberg, and C.-M. Chan, *Low Energy Electron Diffraction*, edited by G. Ertl and R. Gomer, Springer Series in Surface Science Vol. 6 (Springer, Berlin, 1986).
[30] U. Thumm and J. S. Briggs, Nucl. Instrum. Methods Phys. Res. B **43**, 471 (1989).
[31] C. J. Joachain, *Quantum Collision Theory* (North-Holland, Amsterdam, 1975).
[32] C. Kittel, *Introduction to Solid State Physics*, 3rd ed. (Wiley, New York, 1966).
[33] J. Berakdar (unpublished).
[34] M. Abramowitz and I. Stegun, *Pocketbook of Mathematical Functions* (Deutsch-Verlag, Frankfurt, 1984).